INTERNATIONAL JOURNAL OF MEDICAL SCIENCE AND DENTAL HEALTH
(ISSN: 2454-4191)
www.ijmsdh.org (2026)

Check for updates

Received: 09 Sep 2026
Revised: 27 Sep 2026
Accepted: 01 Oct 2026
Published: 15 Oct 2026

Volume 12 Issue 10, 2026
Page No - 26-33
DOI - 10.55640/ijmsdh-12-10-04

Article Citation: Mohammed, M. J. (2026). Numerical Traceability and High-Load Response Departure in Finite Element Analysis of an Implant-Supported Haybrid Ceramic Crown. International Journal of Medical Science and Dental Health, 12(10), 26-33. https://doi.org/10.55640/ijmsdh-12-10-04

Copyright: © 2026 The Authors. Published by IJMSDH under the Creative Commons CC BY License

Numerical Traceability and High-Load Response Departure in Finite Element Analysis of an Implant-Supported Haybrid Ceramic Crown

Marwa J. Mohammed
College of Biomedical Engineering, University of Technology – Iraq

***Corresponding author:**
marwa.j.mohammed@uotechnology.edu.iq

Abstract

Background: Finite element analysis (FEA) is widely used to examine stress and deformation in dental restorations. However, a numerical interpretation is most convincing when the underlying geometry, boundary conditions, mesh, contact definitions, and solver settings can be traced clearly. This study compares two ANSYS configurations of an implant-supported hybrid ceramic crown and examines whether the observed numerical differences can be connected to documented model features.

Methods: Two three-dimensional static-structural configurations, designated Configuration A (nominal 120) and Configuration B (nominal 160), were analyzed under vertical loads of 200, 400, 600, 800, 1000, 1200, and 1400 N. Maximum principal stress, maximum principal elastic strain, equivalent (von Mises) stress, and total deformation were obtained from the ANSYS output tables. Before the numerical responses were compared, the available geometry summaries, body volumes, node and element counts, contacts, loading history, result scoping, and solver settings were checked for consistency. B/A ratios and ordinary least-squares load-response fits were then used as descriptive measures; no inferential hypothesis testing was performed.

Results: The reviewed model-summary fields were the same in both configurations, including an overall model volume of 877.68 mm^3, a cement-body volume of 8.1156 mm^3, 729,292 nodes, 448,331 elements, three active bonded contacts, and Large Deflection set to Off. Configuration A showed an almost proportional response across the full loading range. Configuration B followed a similar pattern up to 800 N, but the maximum principal stress then rose from 309.89 MPa at 800 N to 1319.1 MPa at 1000 N, 7919.3 MPa at 1200 N, and 12460 MPa at 1400 N. Equivalent stress reached 12835 and 13347 MPa at

1200 and 1400 N, respectively, whereas total deformation remained close to proportional and reached 0.17829 mm at 1400 N. This upper-load departure is compatible with a localized and/or numerically sensitive response requiring verification, rather than with a demonstrated failure mechanism.

Conclusions: The two configurations support a focused assessment of load-response departure and numerical traceability. Because the reviewed geometry and mesh fields are indistinguishable between them, the upper-load change cannot be attributed to the nominal labels alone. The main contribution of this analysis is to quantify the departure from the lower-load pattern and to show why extreme FEA maxima should not be given a causal interpretation unless the underlying model difference can be demonstrated independently.

Keywords: finite element analysis; dental implant; hybrid ceramic crown; numerical verification; model traceability; stress analysis; computational reproducibility.

1. Introduction

Finite element analysis (FEA) is widely used in dental and implant biomechanics because it can estimate internal stress, strain, and deformation fields that are difficult to measure directly. At the same time, the value of an FEA result depends strongly on how the model was constructed and on the extent to which that model has been verified and validated [1–6]. Dental FEA can be especially sensitive to choices involving nonlinear behavior, contact definitions, material properties, mesh construction, and boundary conditions [7–10]. For crown systems, both experimental and computational studies have shown that restorative and luting-material properties can influence load-bearing behavior and stress distribution [11–13,17,19]. Work examining cement-space conditions also shows that a nominal spacer or cement-thickness setting should not automatically be treated as proof of the final geometry unless that geometry has been independently confirmed [14–16,18].

A plausible numerical result is not, by itself, evidence of computational credibility. Verification asks whether the mathematical model has been solved correctly, whereas validation asks whether the model is an adequate representation of the physical system for its intended purpose [1,5,6]. This distinction is important in dental biomechanics, where stress maps may change with contact formulation, constitutive assumptions, mesh density, boundary constraints, or result scoping [3,7–10,20]. For that reason, any FEA investigation should establish what parts of the model can actually be traced before a physical mechanism is assigned to differences between configurations.

This study therefore examined two ANSYS configurations of an implant-supported hybrid ceramic crown. The reviewed model summaries showed the same overall geometry dimensions, body volumes, mesh population, contacts, loading history, and principal solver settings. Here, numerical traceability means the ability to connect a reported numerical difference to a documented and independently identifiable difference in geometry, material definition, loading, contact formulation, mesh, solver settings, or result scoping. Rather than assuming that the nominal labels represent verified physical differences, the two configurations are treated as Configuration A and Configuration B and their load-response patterns are examined directly. The study had three objectives: (i) to compare load-dependent maximum principal stress, maximum principal elastic strain, equivalent stress, and total deformation between Configurations A and B; (ii) to describe the load range over which their response patterns begin to separate; and (iii) to determine whether the available model documentation is sufficient to support a causal explanation for the observed numerical differences.

2. Materials and Methods

2.1 Finite-element configurations and study scope

Two ANSYS 18.0 static-structural configurations were included. Their nominal identifiers corresponded to 120 and 160, but the analysis did not assume that these labels represented verified geometric differences. They are therefore referred to as Configuration A and Configuration B throughout the manuscript. All numerical values reported here were obtained directly from the ANSYS output tables associated with the two configurations.

Each configuration consisted of a three-body crown-cement-implant assembly solved as a three-dimensional static structural analysis in Mechanical APDL. The model documentation lists the material assignments as Titanium Alloy, “up”, and cement. However, complete material-property tables for everybody were not available in the documentation used for the present analysis. Missing material constants were therefore not inferred or reconstructed.

2.2 Model summary and traceability review

Before the stress results were compared, the available model documentation was reviewed. Table 1 summarizes the parameters that could be examined directly in both configurations. This step was included to determine whether the observed numerical differences could reasonably be linked to a documented model difference.

Table 1. Model summary for Configurations A and B.

Parameter	Configuration A (nominal 120)	Configuration B (nominal 160)
Overall bounding box (mm)	11.946 × 12.65 × 12.011	11.946 × 12.65 × 12.011
Total model volume (mm³)	877.68	877.68
Bodies	3	3
Cement-body volume (mm³)	8.1156	8.1156
Nodes	729,292	729,292
Elements	448,331	448,331
Active contacts	3	3
Contact type	Bonded	Bonded
Large deflection	Off	Off

The documented model parameters allowed direct comparison of the overall geometry dimensions, cement-body volume, mesh counts, contact count and type, loading history, and the large-deflection setting between Configurations A and B. These parameters were consistent across the two configurations. Additional settings that were not retained in sufficient detail for independent re-verification were not used as a basis for explaining the observed stress differences. Accordingly, agreement in the documented parameters should not be interpreted as proof that every underlying model setting was identical.

2.3 Loading and extracted outcomes

Both configurations used the same seven-level vertical loading history: 200, 400, 600, 800, 1000, 1200, and 1400 N. The load table shows the force acting in the negative global Y direction, with zero X and Z components. The outcomes extracted for comparison were maximum principal stress (MPa), maximum principal elastic strain (mm/mm), equivalent (von Mises) stress (MPa), and total deformation (mm). In both configurations, the reported result objects were scoped by Geometry Selection to one body. The principal-strain tables also identify Geom2 as the location of the reported maximum. Because the editable ANSYS project was unavailable, any underlying named selection or hidden scoping definition beyond the visible output could not be reconstructed independently.

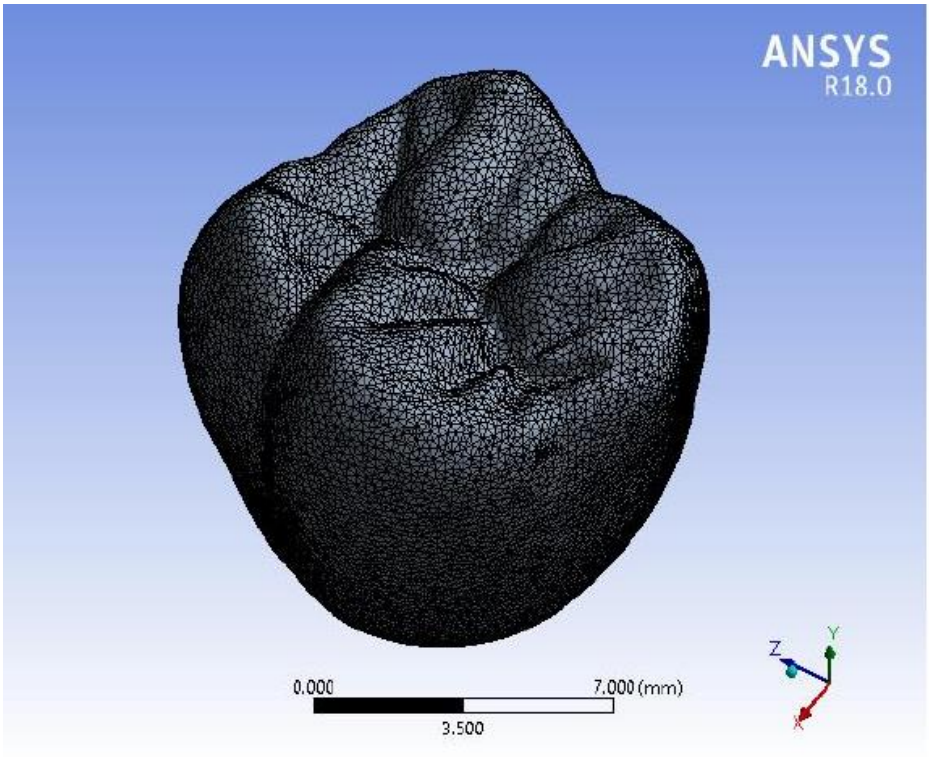

Figure 1. Representative finite-element mesh used in the analysis.

2.4 Analytical approach

The numerical outputs are deterministic simulation results rather than replicated biological or experimental observations. Values were transcribed from the ANSYS output tables and checked against the corresponding plots. B/A ratios were calculated at each load level. Ordinary least-squares fits, with the intercept estimated freely rather than forced through zero, were used only to describe load-response proportionality; R^2 was calculated as 1 - SSE/SST. Calculations were performed in Python 3.13.5 using simple scripted arithmetic and least-squares operations. For Configuration B, proportionality at lower loads was assessed over 200–800 N for principal stress and principal strain because the response changed clearly above this range. No inferential hypothesis testing was applied, and the analysis was not used to assign the observed departure to a biological, material, or geometric mechanism.

3. Results

3.1 Maximum principal stress

Table 2. Maximum principal stress in Configurations A and B.

Load (N)	Configuration A (MPa)	Configuration B (MPa)	B/A ratio
200	66.019	77.506	1.17
400	132.040	155.040	1.17
600	198.060	232.510	1.17
800	264.080	309.890	1.17
1000	330.090	1319.100	4.00
1200	396.110	7919.300	19.99
1400	462.130	12460.000	26.96

Configuration A showed an approximately proportional principal-stress response from 200 to 1400 N, with a fitted slope of about 0.33009 MPa/N ($R^2 > 0.9999$). Configuration B followed a similar proportional pattern between 200 and 800 N, with a low-load slope of about 0.38731 MPa/N. Across this range, the B/A ratio remained close to 1.17. At 1000 N the ratio increased to 4.00, and it rose further to 19.99 at 1200 N and 26.96 at 1400 N, indicating a clear departure from the lower-load pattern.

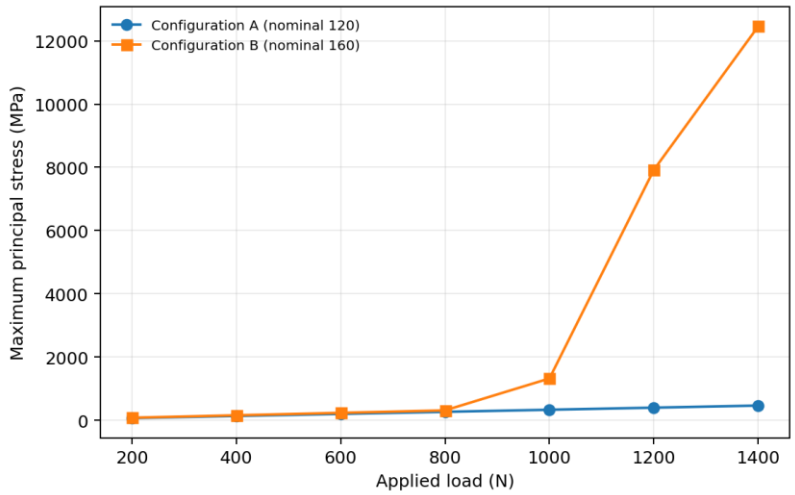

Figure 2. Maximum principal stress versus applied load. Configuration B shows a marked departure from the low-load trend beginning at 1000 N.

3.2 Maximum principal elastic strain

Table 3. Maximum principal elastic strain in Configurations A and B.

Load (N)	Configuration A	Configuration B	B/A ratio
200	0.002412	0.003204	1.33
400	0.004824	0.006406	1.33
600	0.007236	0.009607	1.33
800	0.009649	0.012807	1.33
1000	0.012061	0.038628	3.20
1200	0.014473	0.232330	16.05
1400	0.016885	0.368120	21.80

The strain ratio was also stable at lower loads, remaining close to 1.33 from 200 to 800 N. It increased to 3.20 at 1000 N, 16.05 at 1200 N, and 21.80 at 1400 N. The largest reported local principal elastic strain in Configuration B was 0.36812 at 1400 N. Because Large Deflection was set to Off in the present analysis, this local maximum should be interpreted cautiously under a small-deformation formulation. This high local strain value should be interpreted cautiously.

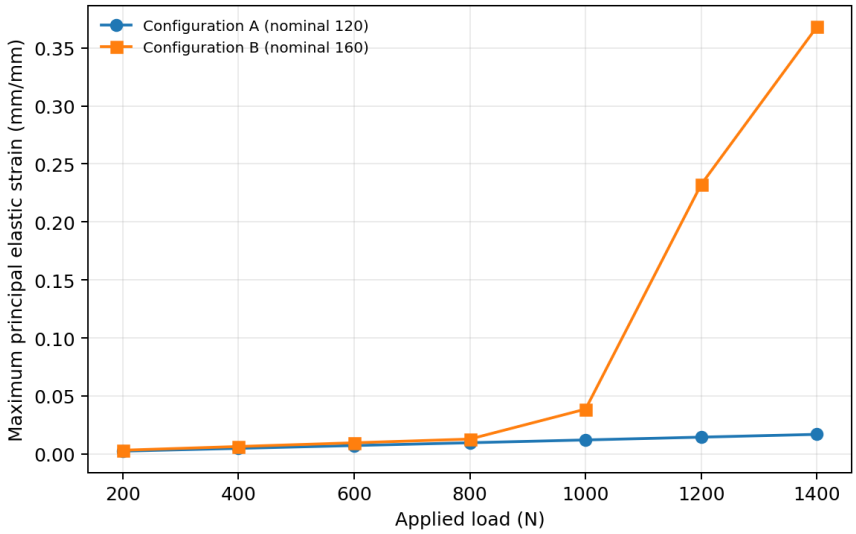

Figure 3. Maximum principal elastic strain versus applied load.

3.3 Equivalent stress and total deformation

Table 4. Equivalent stress, equivalent-stress ratio, and total deformation.

Load (N)	Equivalent stress A (MPa)	Equivalent stress B (MPa)	Eq. stress B/A	Deformation A (mm)	Deformation B (mm)
200	146.96	191.82	1.31	0.02475	0.02548
400	292.82	382.22	1.31	0.04951	0.05096
600	438.57	572.38	1.31	0.07426	0.07644

Load (N)	Equivalent stress A (MPa)	Equivalent stress B (MPa)	Eq. stress B/A	Deformation A (mm)	Deformation B (mm)
800	584.21	762.32	1.30	0.09901	0.10193
1000	729.75	973.41	1.33	0.12377	0.12739
1200	875.18	12835.00	14.67	0.14852	0.15285
1400	1020.50	13347.00	13.08	0.17327	0.17829

Equivalent stress in Configuration A rose smoothly from 146.96 MPa at 200 N to 1020.5 MPa at 1400 N. In Configuration B, the equivalent-stress B/A ratio remained within approximately 1.30–1.33 from 200 to 1000 N. A much larger change appeared at 1200 N, where the ratio reached 14.67, and remained high at 13.08 at 1400 N as the reported maxima reached 12835 and 13347 MPa. These values are numerical maxima from the present analysis and should not be treated as validated material-failure stresses. Total deformation, in contrast, remained close to proportional in both configurations. At each load level, Configuration B was approximately 2.9% higher than Configuration A, reaching 0.17829 mm compared with 0.17327 mm at 1400 N.

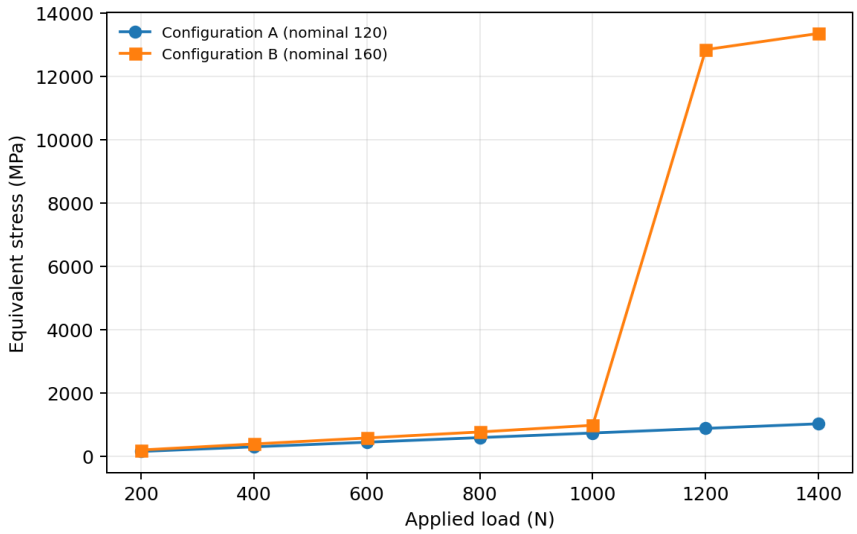

Figure 4. Equivalent (von Mises) stress versus applied load.

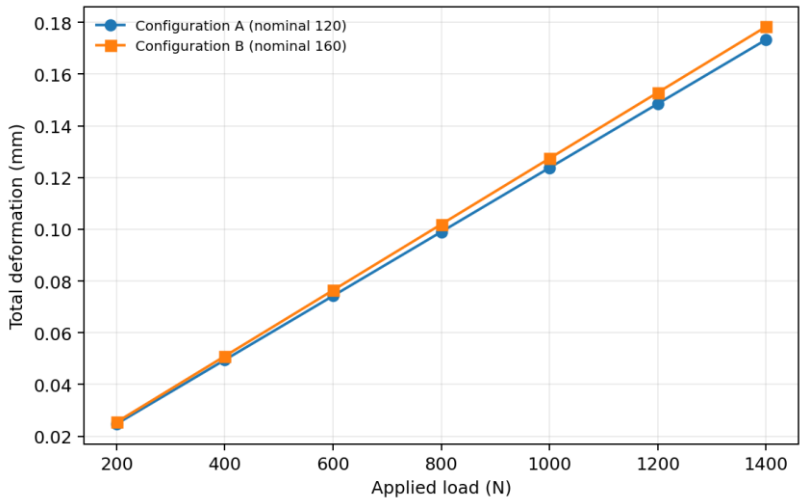

Figure 5. Total deformation versus applied load. Global deformation remains close to proportional with load despite the upper-load departure in local stress maxima in Configuration B.

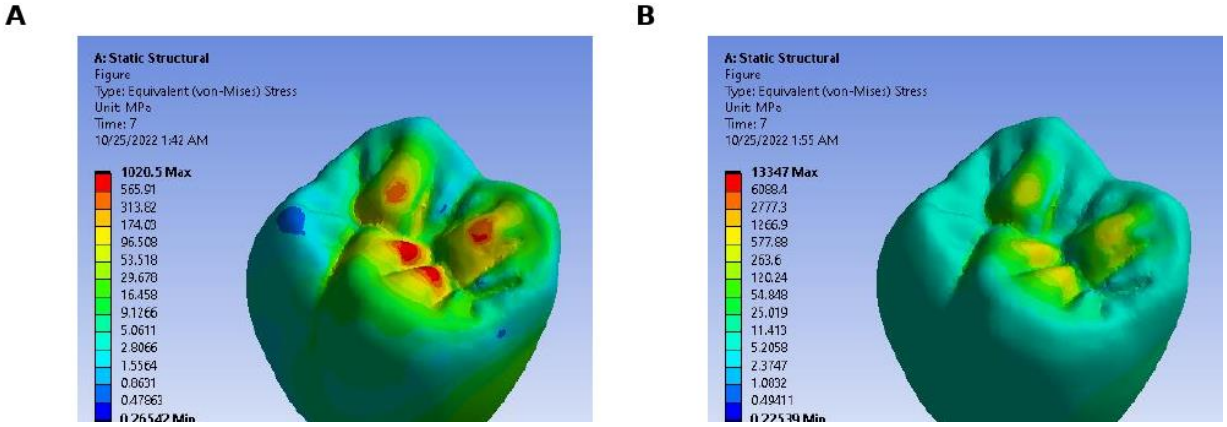

Figure 6. Equivalent-stress contour outputs at the 1400-N step for Configuration A (left) and Configuration B (right).

Each ANSYS image uses its native contour scale; therefore, color differences must not be interpreted quantitatively across panels. Quantitative comparison should rely on the numerical maxima in Table 4. For localization only; not for cross-panel magnitude comparison.

4. Discussion

The main finding is not an effect of the nominal labels themselves, but a clear difference in the load-response pattern of two finite-element configurations whose reviewed model-summary fields are otherwise indistinguishable. Configuration A remained approximately proportional across the investigated loads. Configuration B behaved similarly at low and moderate loads, but its reported local stress and principal-strain maxima rose sharply at the upper loading levels, while total deformation continued to scale almost proportionally with load.

Several explanations could account for the combination of very large local stress or strain maxima and a comparatively smooth global deformation response. These include a highly localized stress concentration, sensitivity to contact or constitutive assumptions that are not visible in the available output, result-scoping effects, or other numerical behavior that could only be diagnosed by re-solving the original model. In principle, a local maximum may change substantially without a similar change in deformation of the whole assembly; however, the available output does not allow that localization mechanism to be confirmed. Contact formulations and nonlinear assumptions are known sources of sensitivity in dental FEA [7,8], while broader reviews also identify material definition, mesh, boundary conditions, and model simplifications as important determinants of calculated stress fields [3,9,10]. The present data do not allow these possibilities to be separated. The upper-load response is therefore treated as a result requiring verification rather than as evidence of structural collapse or a defined material-failure mechanism. The lack of a traceable geometric difference is central to this interpretation. In both configurations, the reviewed fields show the same overall bounding box, total model volume, cement-body volume, node and element counts, three active bonded contacts, and the same large-deflection setting. A causal claim about a nominal design variable would require that variable to be demonstrably different in the underlying model. This position is consistent with computational-model credibility literature, which emphasizes verification, validation, transparent model definition, and comparison with an appropriate physical or experimental quantity before simulation output is given predictive meaning [1,5,6,20].

The external dental literature provides useful context for this methodological interpretation. Experimental studies have linked restorative and cement properties with crown loading capacity [11,12], while failure-load and FEA studies show that calculated stress fields depend on the modeled restoration, cement, loading conditions, and structural interactions [13,17–19]. Studies based on micro-CT or explicit cement-space variation also show that cement-space geometry is measurable and that nominal spacer settings, cement type, and actual internal fit are not interchangeable concepts [14–16,18]. Together, these findings reinforce the need to verify the model variable itself before numerical differences are attributed to it. For this reason, the present results should not be used to recommend a clinical cement-space value, define a failure threshold, or claim that one nominal configuration is superior to the other. Their value is methodological. The analysis shows how two finite-element configurations can produce sharply different local maxima even when the high-level documented fields appear the same, and why nominal labels alone are not enough to support a causal biomechanical interpretation.

5. Conclusions

The present analysis identified a pronounced departure from the lower-load response pattern in Configuration B at the upper loading levels. Maximum principal stress, maximum principal elastic strain, and equivalent stress increased sharply, whereas total deformation remained nearly proportional to load. Because the reviewed model summaries show the same geometry dimensions, cement-body volume, mesh population, contact count, and major solver settings, the observed change cannot be assigned causally to the nominal labels. The study therefore offers a model-traceability and computational-credibility perspective: extreme local FEA maxima should be treated as results requiring verification until the model variable, scoping

definition, or numerical condition responsible for the difference can be demonstrated independently.

References

1. American Society of Mechanical Engineers. ASME V&V 40-2018: Assessing Credibility of Computational Modeling through Verification and Validation: Application to Medical Devices. New York: ASME; 2018.
2. Geng JP, Tan KB, Liu GR. Application of finite element analysis in implant dentistry: a review of the literature. J Prosthet Dent. 2001;85(6):585-598. doi:10.1067/mpr.2001.115251.
3. Falcinelli C, Valente F, Vasta M, Traini T. Finite element analysis in implant dentistry: state of the art and future directions. Dent Mater. 2023;39(6):539-556. doi:10.1016/j.dental.2023.04.002.
4. Reddy MS, Sundram R, Abdemagyd HAE. Application of finite element model in implant dentistry: a systematic review. J Pharm Bioallied Sci. 2019;11(Suppl 2):S85-S91. doi:10.4103/JPBS.JPBS_296_18.
5. Chang Y, Tambe AA, Maeda Y, Wada M, Gonda T. Finite element analysis of dental implants with validation: to what extent can we expect the model to predict biological phenomena? A literature review and proposal for classification of a validation process. Int J Implant Dent. 2018;4(1):7. doi:10.1186/s40729-018-0119-5.
6. Henninger HB, Reese SP, Anderson AE, Weiss JA. Validation of computational models in biomechanics. Proc Inst Mech Eng H. 2010;224(7):801-812. doi:10.1243/09544119JEIM649.
7. Wakabayashi N, Ona M, Suzuki T, Igarashi Y. Nonlinear finite element analyses: advances and challenges in dental applications. J Dent. 2008;36(7):463-471. doi:10.1016/j.jdent.2008.03.010.
8. Murakami N, Wakabayashi N. Finite element contact analysis as a critical technique in dental biomechanics: a review. J Prosthodont Res. 2014;58(2):92-101. doi:10.1016/j.jpor.2014.03.001.
9. Celik HK, Koc S, Kustarci A, Rennie A. A literature review on the linear elastic material properties assigned in finite element analyses in dental research. Mater Today Commun. 2022;30:103087. doi:10.1016/j.mtcomm.2021.103087.
10. Prados-Privado M, Martínez-Martínez C, Gehrke SA, Prados-Frutos JC. Influence of bone definition and finite element parameters in bone and dental implants stress: a literature review. Biology (Basel). 2020;9(8):224. doi:10.3390/biology9080224.
11. Rohr N, Coldea A, Zitzmann NU, Fischer J. Loading capacity of zirconia implant supported hybrid ceramic crowns. Dent Mater. 2015;31(12):e279-e288. doi:10.1016/j.dental.2015.09.012.
12. Rohr N, Märtin S, Fischer J. Correlations between fracture load of zirconia implant supported single crowns and mechanical properties of restorative material and cement. Dent Mater J. 2018;37(2):222-228. doi:10.4012/dmj.2017-111.
13. Campos RE, Soares PV, Versluis A, de O Júnior OB, Ambrosano GMB, Nunes IF. Crown fracture: failure load, stress distribution, and fractographic analysis. J Prosthet Dent. 2015;114(3):447-455. doi:10.1016/j.prosdent.2015.02.023.
14. Dauti R, Lilaj B, Heimel P, Moritz A, Schedle A, Cvikl B. Influence of two different cement space settings and three different cement types on the fit of polymer-infiltrated ceramic network material crowns manufactured using a complete digital workflow. Clin Oral Investig. 2020;24(6):1929-1938. doi:10.1007/s00784-019-03053-1.
15. Dauti R, Cvikl B, Lilaj B, Heimel P, Moritz A, Schedle A. Micro-CT evaluation of marginal and internal fit of cemented polymer infiltrated ceramic network material crowns manufactured after conventional and digital impressions. J Prosthodont Res. 2019;63(1):40-46. doi:10.1016/j.jpor.2018.04.005.
16. Mounica Y, Behera S, Arunachalam S, Srikanth L, Deepthi MN, Susmita M. Influence of different cements and cement thickness on the stress distribution under occlusal surfaces of porcelain-fused-to-metal and porcelain-fused-to-zirconium crowns: a finite element analysis. J Contemp Dent Pract. 2022;23(12):1224-1229. doi:10.5005/jp-journals-10024-3448.
17. Ha SR. Biomechanical three-dimensional finite element analysis of monolithic zirconia crown with different cement type. J Adv Prosthodont. 2015;7(6):475-483. doi:10.4047/jap.2015.7.6.475.
18. Ha SR, Kim SH, Lee JB, Han JS, Yeo IS, Yoo SH, Kim HK. Biomechanical three-dimensional finite element analysis of monolithic zirconia crown with different cement thickness. Ceram Int. 2016;42(13):14928-14936. doi:10.1016/j.ceramint.2016.06.133.
19. Ausiello P, Di Lauro AE, Tribst JPM, Watts DC. Stress distribution in resin-based CAD-CAM implant-supported crowns. Dent Mater. 2023;39(1):114-122. doi:10.1016/j.dental.2022.12.001.
20. Waldecker M, Rues S, Rammelsberg P, Bömicke W. Validation of in-vitro tests of zirconia-ceramic inlay-retained fixed partial dentures: a finite element analysis. Dent Mater. 2019;35(3):e53-e62. doi:10.1016/j.dental.2019.01.017.